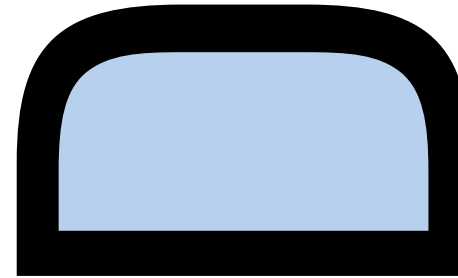


WHITE PAPER SERIES / EDITION 1



AUTO-ID LABS

BUSINESS PROCESSES & APPLICATIONS
SOFTWARE & NETWORK
HARDWARE

AUTOIDLABS-WP-HARDWARE-015



**UHF Band RFID Readability and Fading
Measurements in Practical Propagation
Environment**

Jin Mitsugi

Auto-ID Lab Japan

www.autoidlabs.org



1. Introduction

UHF passive RFID system has gathered significant interests from industrial as well as technical and administrative body. Technical standardization and local radio regulations have been under development accordingly. In Japan, a number of experiments have been carried out to evaluate the real benefit of introducing UHF passive RFID systems. The basic advantage of UHF passive RFID system, compared with other frequency bands, 13.56MHz and 2.45GHz, is its long range communication between the reader and tags. It was experienced; however, sufficient communication range might not be available in not few practical situations. Since the communication range of passive RFID system is usually dominated by the power supplied by a reader in the form of RF signal, direct measurement of RF signal is expected to provide further understanding of the radio layer performance. For this purpose, the author had fabricated a folded dipole antenna, called tag probe, to measure the field strength of the reader emission in place of tags.

One of the motivations to fabricate the tag probe is to evaluate the practical fading of the UHF (950MHz) passive RFID. Particular interest is on the effect of frequency shifting to dislocate the field nulls generated by the fading. At the occasion of a research forum of Keio University, Auto-ID Lab Japan carried out experiments on the fading of UHF passive RFID. This paper presents the preparation and the outcome of the experiments.

After reports on the experimental setup and tag readability for the participant management for the research forum, the practical fading for a gate application in large scale exhibition were reported in this paper. Field nulls were observed in the experiment and the frequency dependency is also reported. The results are discussed with a comparison with analytical multipath model.

2. Experimental setup

2.1 RFID system and antenna orientation

To minimize the possible interference against the existing radio services, cellular phone system, the boresight of RFID antenna is oriented downwards with slant angle of up to 10degree. With this configuration, the horizontal emission from RFID can be reduced at least by 13dB. The suppression value can be obtained from the antenna pattern of the RFID reader antenna shown in Figure 1 and Figure 2.

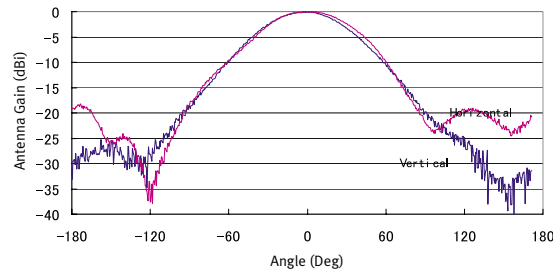


Fig. 1: RFID antenna pattern

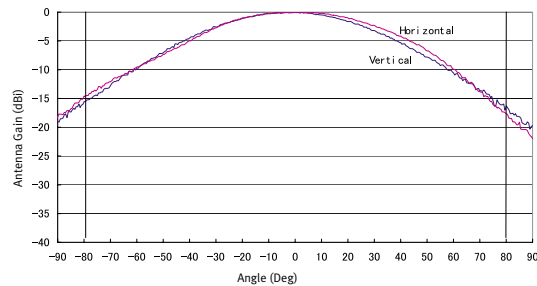


Fig. 2 RFID antenna pattern close up

The dimension of the experimental RFID gate is shown in Figure 3. Two antennas, antenna 1 and antenna 2 are used in the experiment.

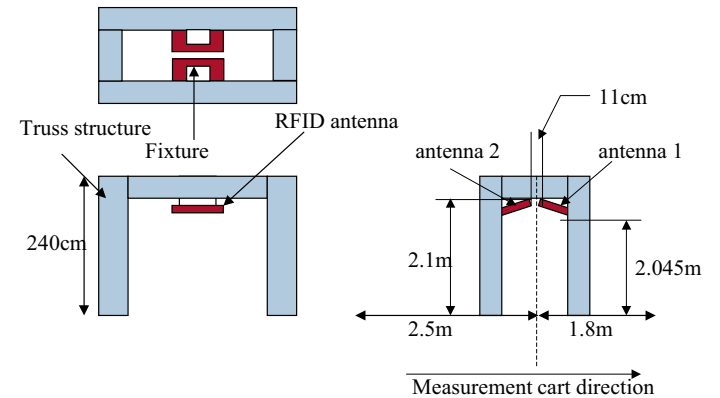


Fig. 3: RFID system setup

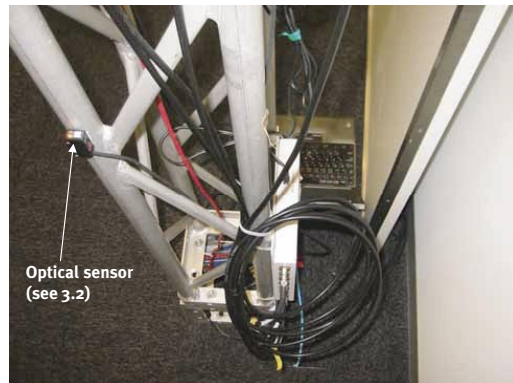
The picture of the actual setup are shown from Figure 4 to Figure 6.



Fig. 4: RFID system setup



Fig. 5: RFID antenna configuration



Optical sensor
(see 3.2)

Fig. 6: RFID reader

2.2 Measurement cart description

Fading effect is measured by receiving RF signal emission from signal generator by dipole antennas and spectrum analyzer. The measured data is saved in data recorder. The schematic of the measurement is shown in Figure 7.

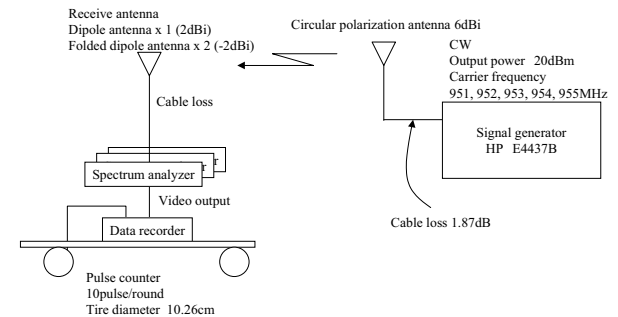


Fig. 7: Fading measurement

Loss of the cables between receiving antennas and spectrum analyzer were listed in Table 1.

Antenna	Spectrum analyzer	Loss	Height from floor
Dip ole ante nna	8563E	1.43dB	105(cm)
Tag probe 1	8560A	1.18dB	136(cm)
Tag probe 2	8564E	1.25dB	74(cm)

The outlook of the measurement cart is shown in Figure 8.

Table 1 Tag probe and dipole antenna connection

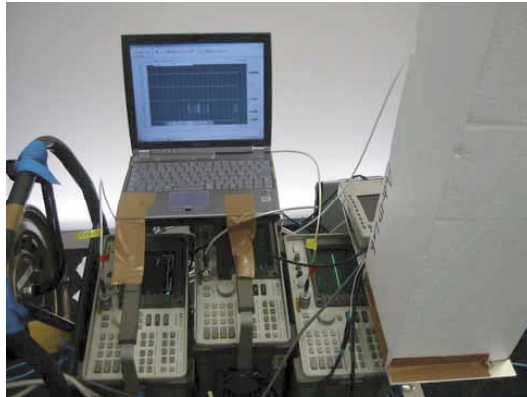


Figure 8: Measurement cart

Spectrum Analyzer setup is summarized in Table 2.

RBW	3kHz
VBW	3kHz

Table 2: Spectrum Analyzer Setup

2.3 Pulse encoder calibration

The measurement cart furnishes a pulse encoder to measure the cart position by counting the rotation of one of the wheel. One rotation of the wheel generates ten pulses. The outer diameter of the wheel is derived by measure the actual moving line length of the cart. The outer diameter is 10.26cm. The sampling rate, over 100Hz, need to be implemented not to lose pulses generated.

2.4 Spectrum analyzer calibration

The dynamic power level fluctuation due to the fading was measured using zero span output of spectrum analyzer. Since the

correlation between zero span video output level and the actual power level depends on the spectrum analyzer, the calibration was done prior to the testing. The fundamental setting of three spectrum analyzer, HP8594, HP8563E and HP8560A is as shown in Table 3.

Parameter	Setting
RBW	3kHz
VBW	3kHz
Attenuation	10dB
Reference level	0dBm

Table 3: Spectrum analyzer setting for zero span measurement

The calibration is measured by using a variable attenuator between a signal generator and the spectrum analyzer as shown in Figure 9.

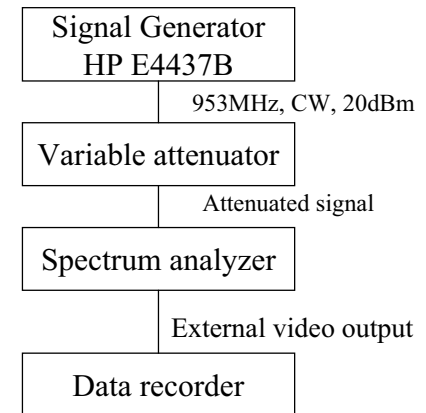


Fig. 9: Spectrum analyzer calibration set up

The calibration values are shown in from Table 4 to Table 6.

Input to spectrum analyzer (dBm)	External video output(V)
-0.40	0.98
-10.00	0.85
-20.30	0.72
-30.30	0.59
-40.20	0.46
-50.20	0.33
-60.00	0.20
-68.70	0.09

Table 4: Spectrum analyzer video output calibration (8954E)

Input to spectrum analyzer (dBm)	External video output(V)
0.50	2.05
-9.50	1.86
-19.50	1.66
-29.50	1.46
-39.50	1.26
-49.67	1.06
-59.50	0.87
-68.50	0.69

Table 5: Spectrum analyzer video output calibration (8563E)

Input to spectrum analyzer (dBm)	External video output(V)
0.17	2.03
-9.67	1.84
-19.67	1.64
-29.83	1.44
-39.83	1.25
-50.00	1.05
-60.00	0.85
-68.60	0.68

Table 6: Spectrum analyzer video output calibration (8560A)

The linear approximation of the calibrated values are shown from Figure 10 to Figure 12. It can be observed that the video output is fairly proportional to the input RF power for every three spectrum analyzer.

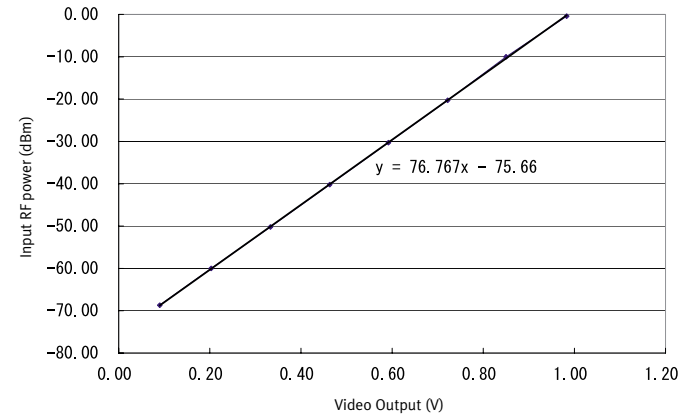


Fig. 10: Spectrum analyzer 8594E calibration

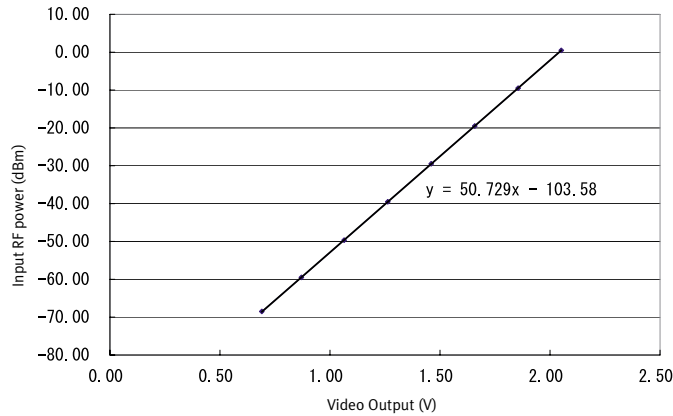


Figure 11: Spectrum analyzer (8563E) calibration

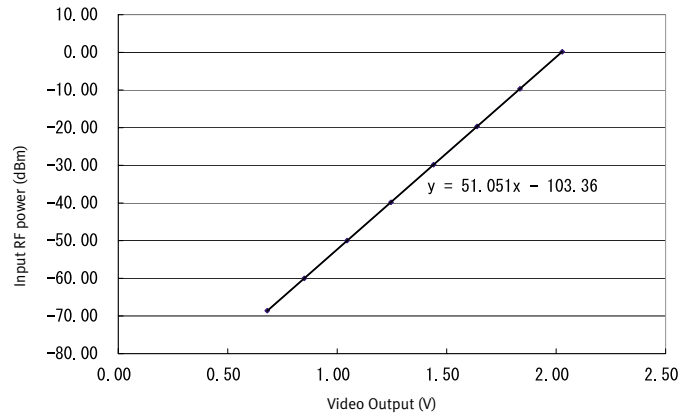


Figure 12: Spectrum analyzer (8560A) calibration

2.5 RFID reader output calibration

As stated in the following sections, the RFID reader is remotely controlled through a firmware implemented in the reader. The output level of the RFID reader can be adjusted from level 0x00 to level 0xFF. Since the actual output level and the hexagonal input is not known, the relationship is measured. A coupler, -20dB divider, is used to separate the TX signal as shown in Figure 13.

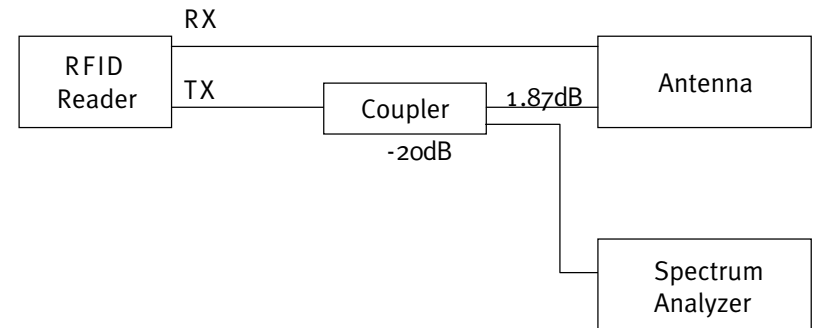


Fig.e 13: RFID reader output level calibration

The measured output and the actual input to the antenna port after coupler compensation and the inclusion of the antenna cable loss is shown in Table 7. In the experiment, the bold figures, namely FF, BB and 77, are employed.

Input level	Direct reading of spectrum analyzer (dBm)	Coupler (-20dB) and cable loss (1.87dB) compensated (dBm)
FF	8.8	27.0
EE	7.5	25.6
DD	7.2	25.3
CC	6.8	25.0
BB	5.0	23.1
AA	4.3	22.5
99	3.3	21.5
88	2.3	20.5
77	0.0	18.1
66	-1.3	16.8
55	-4.2	14.0
44	-6.7	11.5
33	-11.5	6.6
22	-22.8	-4.7
11	-47.5	-29.4

Table 7: Reader output level calibration

3. Practical readability of UHF RFID in automatic human count application

3.1 Readability in practical environment

Practical readability was measured in accordance with said three power levels, namely 27dBm, 23.1dBm and 18.1dBm with antenna gain of 6dBi. The readability is counted by successful reader recognition of the three persons repeatedly, 20 times, passing by the gate as shown in Figure 14.



Fig. 1: Measurement of practical readability

The readability in accordance with the output level is summarized in Table 8.

Test case	Person	Output level (EIRP)		
		27dBm (33dBm)	23.1dBm(29.1dB m)	18dB m(24dB m)
Case 1	Person 1	100%(2 0/20)	100%(20/20)	65%(13/20)
	Person 2	100%(2 0/20)	100%(20/20)	75%(15/20)
	Person 3	100%(20/20)	85%(17/20)	10%(2/20)
Case 2	Person 1		100%(2 0/20)	
	Person 2		80%(16/2 0)	
	Person 3		85%(17/2 0)	

Table 8: Practical readability

It is shown that 100% readability can be achieved with 33dBm EIRP emission, while the lower level emission yields degradation of readability. The readability however depends on the person to whom a tag is attached.

3.2 Verification with optical sensor

The readability is verified with the data obtained from optical sensor (Keyence PZ-M51). The optical sensor is installed at a gate and counted the number of people passing by. Since the optical sensor merely detects the blockage of infrared beam between transmitter and receiver, it overestimates the number of a person if the movement of hand or bag of a person is separately detected. The optical sensor may underestimate when two person simultaneously block the infrared beam. Optical sensor involves such source of count errors.

The number of person counted by the optical sensor and RFID for 1000seconds with 10sec interval is shown in Figure 15. In this case the RFID emission power is 500mW.

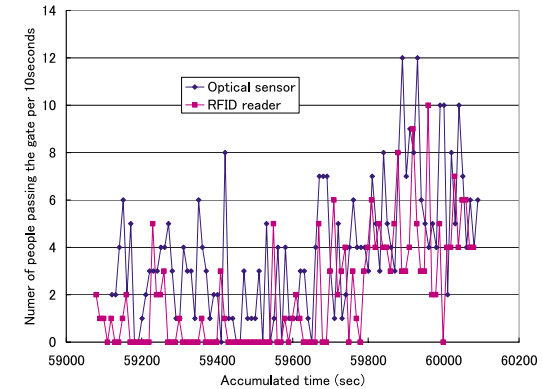


Fig. 15: Verification with optical sensor

It is shown that good agreement is achieved. To filter out the short term difference between RFID and optical sensor due to the clock misalignment, the comparison is retried with 30sec interval (Figure 16).

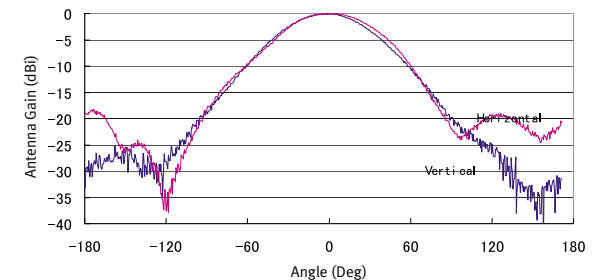


Fig. 16: Verification with optical sensor (30sec. interval)

Profiles of the two data coincide satisfactorily. The remaining difference may be over or undercounting of people with optical sensor and many people, students, do not wear RFID badge.

The verification is also done in different time span and shows another satisfactory agreement.

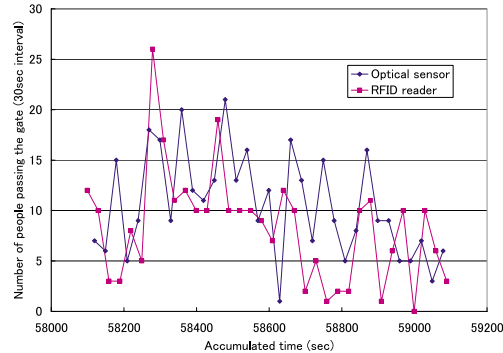


Fig. 17 Verification with optical sensor

4. Fading measurement

Fading is measured by using the measurement cart in an actual noise environment. To minimize the effect of variation of receiving antenna gain, standard dipole and two tag, variation, the horizontal polarization is used in receiving antenna.

4.1 Measured field null positions and frequency dependency

Fading was measured ten times for each carrier frequency. Figure 18 shows the fading data for 951MHz carrier transmitted from antenna 1. As long as the distance is below 2.5m, the fading is fairly consistent against the measurements. Clear field nulls are observed. The intervals of the field null are not constant, though. When the distance is beyond 2.5m, the signal from the antenna is blocked by the operator's body and results in the disturbance.

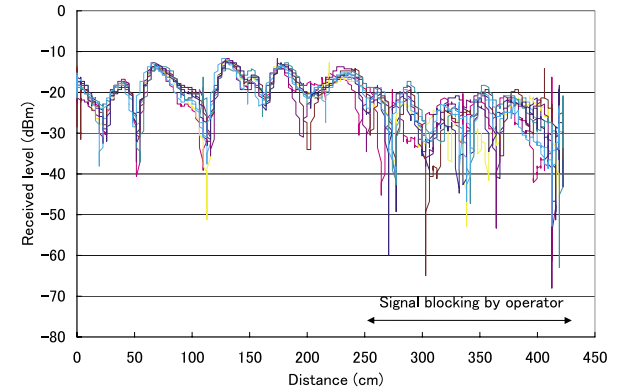


Fig. 18: Fading measurement (951MHz, Ant1, Dipole)

Fading against 953MHz carrier is shown in Figure 19. Again, ten times measurements shows the repeatability of the fading. Clear field nulls are observed at 22, 54, 112, 164 and 199cm.

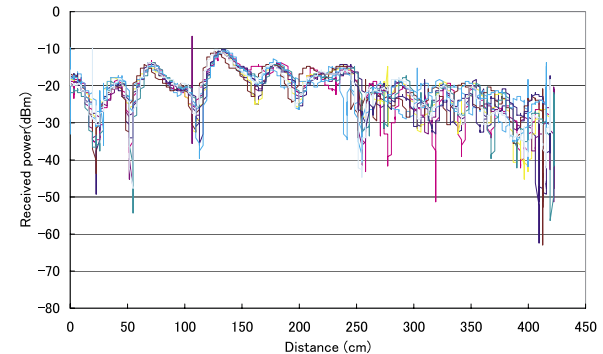


Fig. 19: Fading measurement (953MHz, Ant1, Dipole)

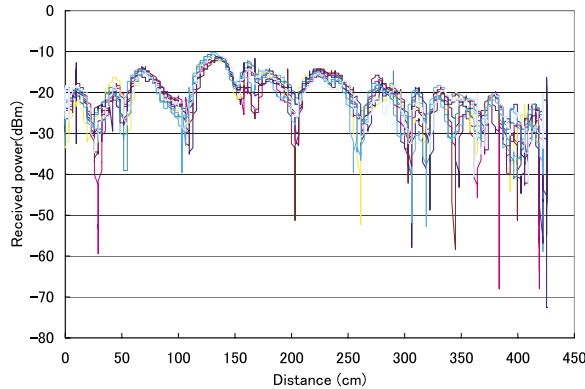


Fig. 20: Fading measurement(955MHz, Ant1, Dipole)

The position of field nulls are summarized as in Table 3. It is shown that the field positions are virtually the same taking into account of the position measurement accuracy 3.2cm.

Frequency(MHz)	Field nulls position (cm)				
	1 st	2nd	3rd	4th	5th
951	19	51	112	161	199
953	22	54	112	161	196
955	29	51	109	157	203

Table 9: Field null positions

With these result, it can be said that there will be field nulls due to multipath fading in UHF band RFID system and the avoidance of the field nulls within a couple of mega hertz frequency band will not provide significant improvement on the reading performance. It should be noted that the fading pattern depends on the environment and polarization.

4.2 Field null dislocation with multiple antennas

RFID system usually supports multiple antennas. It is likely to be able to dislocate the field nulls with different antenna. The fading with antenna1 is measured. For the clarity of the result only one case of fading for each antenna is depicted in Figure 21, although the measurement for antenna 1 was performed for five trials.

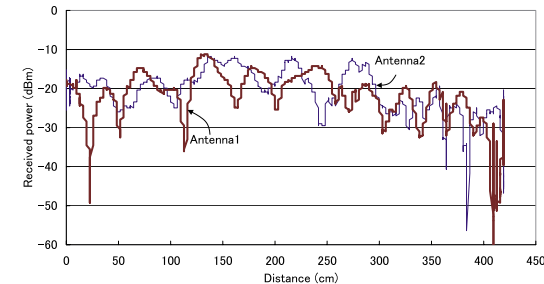


Fig. 21: Fading improvement with multiple antennas

It is shown that the part of the field nulls can be somewhat mutually complementary even with 11cm separation of antennas enabling extended exposure of tags to RF field.

4.3 Readability and power level review

A tag probe is attached to a human as shown in Figure 22 and received level along the gate is measured. The power level was measured six times and the results are shown in Figure 23.



Fig. 22: Tag probe attached to human

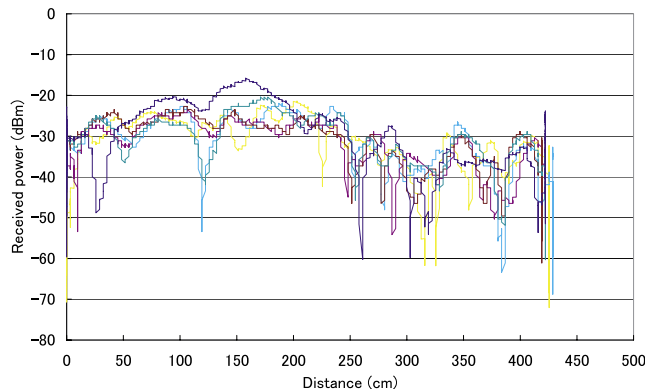


Fig. 23 Tag probe attached to human

In subsection, エラー! 参照元が見つかりません。 it was found that -12dBm received power is equivalent to the minimum tag power requirement when the emission is 30dBm . In this measurement, a signal generator whose emission power is 20dBm was used so that -22dBm line can be regard as the minimum power requirement for tag reading. The minimum power level in accordance with the emission power is summarized in Figure 24.

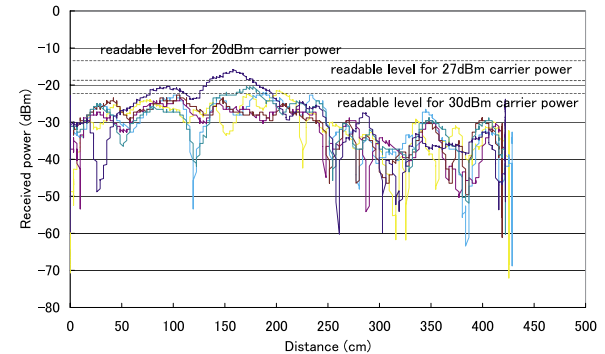


Fig. 24 Received level

If the emission is 30dBm , there is a sufficient time to singulate a tag resulting in the 100% readability which agrees well to Table 8. If the emission is 27dBm , the charge time period is reduced so that the readability will be degraded. If the emission is 20dBm , the readability is significantly degraded. Again, the tendency agrees well to Table 8. To this end, it can be said that it is practical to predict the readability of tags by measuring the power level with tag probe.

4.4 Observations using numerical simulations

From the above experiment, it was shown that the multipath fading is present in practical RFID environment resulting in possible

reading performance degradation. Since the fading environment is different for the usage model and environment, the accurate prediction on what causes the fading, therefore, is not the main issue here. Rather, handling of the field nulls caused by the fading should be discussed while accepting the existence of fading.

Let us first work on the five-path model which will provide us a simple and yet further understanding of the physics. Five-path model fading considering the geometry of the experimental environment, direct path and reflections from the ceiling, floor and side walls, and also the polarization for the experiment geometry is shown in Figure 25. It is shown that the field nulls similar to the experimental results at 0.3m and 2.7m are observed, though experimental data reveals two more nulls at 1.0m and 2.0m reducing the singulation time. This should be because of more than five paths exist in the real situation. We may also need to take into consideration of the exact three dimensional pattern of the receiving antenna if we need to rely on accurate propagation simulation.

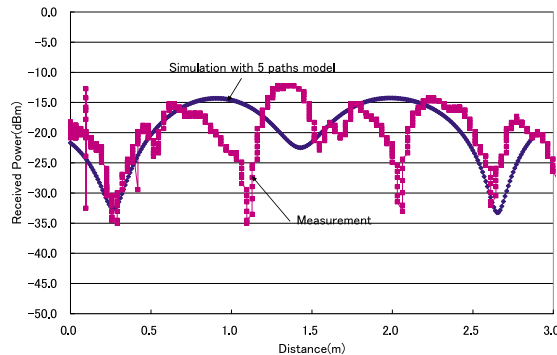


Fig. 25 Five-path model

In another view, it is shown that the fading entails limitation of the reading time when we consider that certain electric power

is needed to power up tags. In fading environment, the received power would fluctuate and provides unstable reading. It could be a major problem for high speed and multiple tag reading.

Frequency dependency of the fading is evaluated with the five path model (Figure 26). for 951MHz, 955MHz and 961MHz. The null shift is, if any, is marginal, which agrees to the experimental result in Table 9 when the available frequency band is a couple of MHz. It is, however, shown that if the available bandwidth could be larger than 10MHz, the field nulls could be dislocated by the size of tags (10cm order).

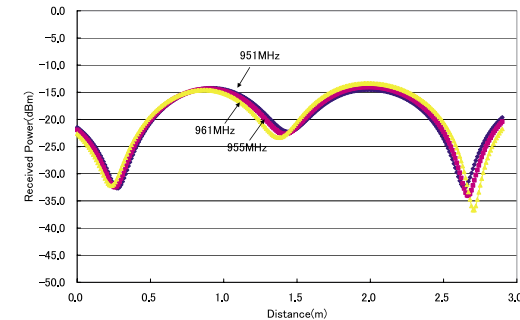


Fig. 26 Frequency dependency of field nulls

5. Conclusions

UHF RFID readability depends on the propagation environment such as tag height and the fading. It is also expected that the dielectric characteristics of the object to which a tag is attached may be significantly changed. Fading in gate-type applications can not be overlooked when we would like to establish high readability



especially for high speed readings of multiple tags. Within the radio regulation environment where a couple MHz could be allocated to UHF RFID, it is unlikely we can satisfactorily dislocate field nulls of fading with frequency shift, like frequency hopping. This is due to the simple fading model of RFID where at least line of sight path needs to be secured for the tag powering entailing short delays. Satisfactory agreement between the measured fading and multipath simulation has not been achieved. We may need to involve detailed geometry of the situation when we fully rely on the propagation simulation to predict the fading environment.



References

- [1] Jin Mitsugi, Peter Cole, Hao Min, “Technical aspects underlying EPCglobal Class1 Generation 2 standardization”, MWE2004, pp.37-44, (2004).
- [2] Palomar Project Deliverable D7, 2002.